Chinese Journal of Chemical Engineering 89 (2026) 324–333

Contents lists available at ScienceDirect

Chinese Journal of Chemical Engineering

journal homepage: www.elsevier.com/locate/CJChE

Full Length Article

Insight into the mechanism of copper on pyrolysis of waste polyurethane: Decrease the activation energy and reduce halogenated compounds

Houyuan Jia [1,#], Jiahui Wang [2,#], Chunyan Feng [3], Siyi Xu [1], Ruitong Gao [1,*], Hui Du [1]

[1] College of Chemistry and Chemical Engineering, Qingdao University, Qingdao 266071, China
[2] College of Life Sciences, Qingdao University, Qingdao 266071, China
[3] Dongying Ecological Environment Service Center of Shandong Province, Dongying 257094, China

ARTICLE INFO

Article history:
Received 2 July 2025
Received in revised form
27 August 2025
Accepted 28 August 2025
Available online 12 September 2025

Keywords:
Waste polyurethane
Cu-assisted pyrolysis
Thermal decomposition kinetics
Pyrolysis mechanism

ABSTRACT

Pyrolysis technology has emerged as a promising method for converting waste polyurethane (WPU) from waste refrigerators into high-value chemicals. In this study, the copper (Cu)-assisted pyrolysis strategy was employed to enhance the thermal degradation efficiency and product quality of WPU. Kinetic analysis revealed that the activation energy (E_a) of the Cu-assisted pyrolysis was 136.64 kJ·mol^{-1} and Cu-assisted pyrolysis was controlled by the combined processes of diffusion, nucleation and phase boundary reactions. Comprehensive product analysis, including gas chromatography–mass spectrometry and thermogravimetric Fourier transform infrared spectroscopy–mass spectrometry suggested that Cu promoted the cleavage of urethane bonds and accelerated the decarboxylation of isocyanates, increasing the yields of aniline and ethanol at lower temperatures. Meanwhile, Cu effectively suppressed the formation of halogenated and heterocyclic compounds by promoting the cleavage of C–X (X = Cl, F) bonds through electron transfer interactions. Thus, the E_a is decreased and the halogenated compounds is reduced. This work provides the theoretical basis for converting waste to high-valued products through co-pyrolysis techniques.

1. Introduction

Polyurethane (PU) is a versatile polymer widely used in various industries such as automotive, construction, furniture, and electronics due to its excellent mechanical properties, flexibility, and thermal stability [1,2]. PU is a polymer synthesized through the condensation of polyols and isocyanates and possesses a recoverable energy value that makes it a potential alternative fuel source in thermal recovery processes [3]. The global PU market was valued at 87.48 billion dollars in 2025 and is projected to reach a valuation of 113.84 billion dollars by 2030 [4]. However, the extensive utilization of PU has resulted in the accumulation of substantial waste polyurethane (WPU), leading to environmental concerns owing to its non-biodegradable nature [5]. At present, WPU is primarily disposed of through landfilling and incineration [6]. Landfills occupy significant land resources, and incineration not only is energy-intensive but also generates secondary pollutants, further burdening the environment [7]. Therefore, developing effective recycling and disposal methods for WPU is crucial.

Pyrolysis, as a potential method for converting WPU into valuable chemicals and fuels, has received widespread attention [8]. During the pyrolysis process, WPU decomposes into small molecules, forming pyrolytic oil and gas in the condensation zone [9]. Pyrolytic oil and gas can be recovered and utilized as high-value fuels and chemicals. Previous studies have indicated that the pyrolysis process of WPU can be described as the cleavage of urethane bonds into isocyanates and polyols [10]. The polyols then further decompose into small molecules, ethers, alkanes, and alkenes, while the isocyanates decompose to form aniline and its derivatives [11]. However, the pyrolysis process also generates heterocyclic compounds and halogenated compounds, which not only reduce the yield of high-value products (such as

* Corresponding author.
E-mail address: gaoruitong@qdu.edu.cn (R. Gao).
# These authors contributed equally to this work.

https://doi.org/10.1016/j.cjche.2025.08.014

ethanol, aniline, and their derivatives) but also exhibit toxic effects on microorganisms and ecosystems [12,13]. Therefore, catalytic pyrolysis is necessary.

Co-pyrolysis, as an effective method to lower decomposition temperature, to improve product selectivity, and to enhance overall process efficiency, has been investigated [14,15]. Gao *et al.* [16] reported that the coexistence of Cu in waste printed circuit boards could change the pyrolysis mechanism function and reduce the apparent activation energy. Cu facilitates the debromination process by preferentially adsorbing and transferring electrons to cleave C–Br bonds, thereby improving the handling efficiency of pyrolysis products. In addition, Liu *et al.* [17] discovered that the *in-situ* catalytic pyrolysis of oily sludge using coal gangue char significantly enhanced the yield and quality of pyrolysis oil and gas, mainly by promoting the cracking of heavy components and facilitating secondary reactions. In a separate study, Liu *et al.* [18] found that microwave co-pyrolysis of textile sludge and furfural residue significantly inhibited the release of nitrogen- and sulfur-containing volatiles, enriched C and H in biochar, and promoted the formation of alkanes, aldehydes, and ketones in the pyrolysis products. These studies demonstrate the great potential of co-pyrolysis strategies in optimizing pyrolysis behavior and product quality. However, little attention has been paid to the synergistic interactions between WPU and Cu during co-pyrolysis, especially regarding the specific mechanisms and effects of Cu on the pyrolysis pathways of WPU. Therefore, further investigation is required to shed light on the underlying mechanism.

This study aims to investigate the effect of Cu-assisted pyrolysis behavior of WPU, with a particular emphasis on decomposition kinetics, product distribution, and reaction mechanisms. By employing various analytical techniques, we will investigate the process of thermal kinetics, the effects of Cu on the chain cleavage of WPU, the formation of intermediates, and the generation of final pyrolysis products. This research will offer important insights into Cu-assisted pyrolysis of WPU and assist in the development of effective recycling methods for WPU.

2. Experimental

2.1. Materials

The WPU utilized in this study originated from waste refrigerators supplied by factories in Qingdao, Shandong Province. As shown in Fig. 1, WPU powder with most of the metal and plastic impurities removed was obtained through dismantling, crushing, mechanical, and electrostatic separation. Finally, polyurethane particles with a particle size of 0.38–0.83 mm were selected for the experiment *via* sieving. The main chemical mass compositions of WPU were carbon (65.02%), oxygen (17.41%), nitrogen (7.01%), hydrogen (6.20%), chlorine (3.56%) and fluorine (0.80%). Cu (Macklin, AR, 99% purity, particle size ~5 μm) was used as received without any further surface modification or pretreatment (Fig. S1, in Supplementary Material). Other chemicals used in the study were analytical grade and were not further purified.

2.2. Experimental procedure

Initially, WPU and Cu were mixed in a 1:0.1 mass ratio as the experimental samples (Fig. 1). Then, the samples were put into alumina crucibles and positioned within a fixed-bed reactor. Next, the fixed-bed reactor was purged with high-purity argon at 50 $ml \cdot min^{-1}$ for 8–12 min to ensure complete removal of air. After that, the pyrolysis reaction was conducted by heating the fixed-bed reactor at 10 $K \cdot min^{-1}$ to 873 K under argon atmosphere, maintaining for 15 min. Finally, the pyrolysis solid was retained within the alumina crucible, while the pyrolysis oil was collected by condenser, and the pyrolysis gas was collected by air collection bag. The yields of pyrolysis solid (X_{solid}), oil (X_{oil}), and gas (X_{gas}) were calculated using Eqs. (1)–(3) as follows:

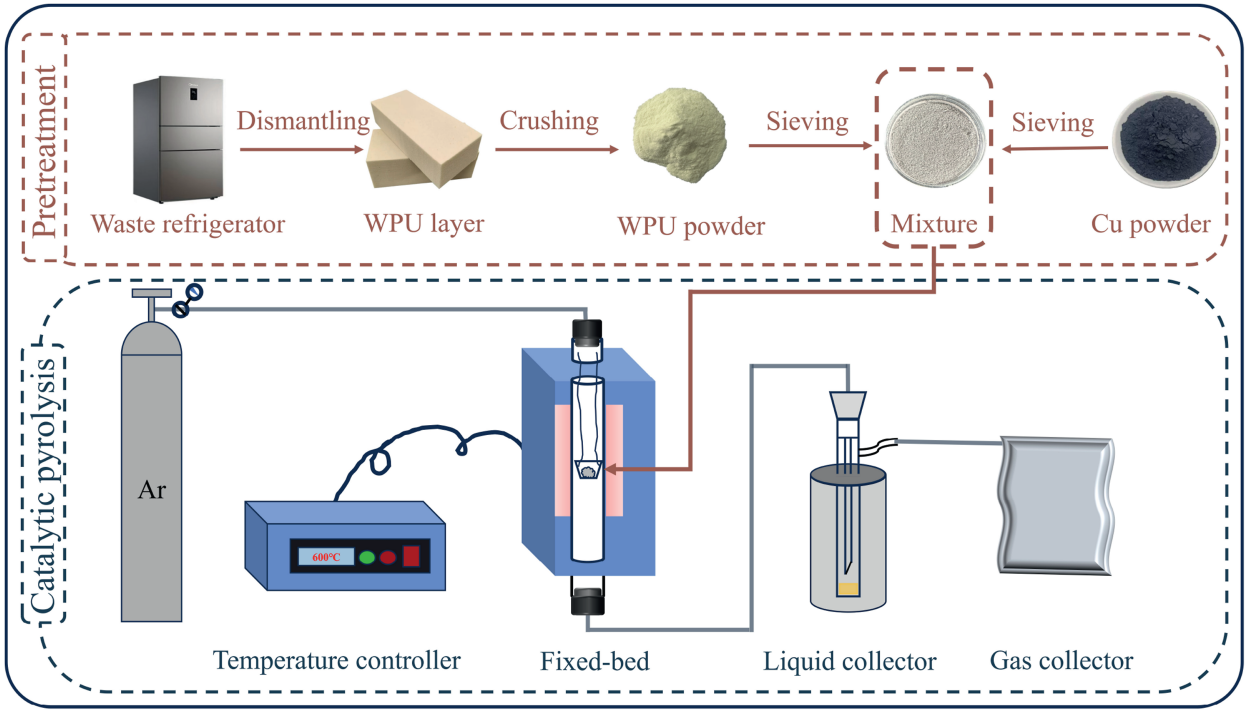

Fig. 1. Flow chart of equipment for Cu-assisted pyrolysis of WPU.

$$X_{\text{solid}} = \frac{m_{\text{solid}}}{m_{\text{sample}}} \times 100\% \tag{1}$$

$$X_{\text{oil}} = \frac{m_{\text{oil}}}{m_{\text{sample}}} \times 100\% \tag{2}$$

$$X_{\text{gas}} = 100\% - X_{\text{solid}} - X_{\text{oil}} \tag{3}$$

where m_{sample}, m_{solid}, m_{oil}, and m_{gas} represent the masses of WPU + Cu, pyrolysis solid, pyrolysis oil, and pyrolysis gas, respectively.

2.3. Pyrolysis kinetics

To elucidate the pyrolysis kinetics, the Friedman method was employed to calculate the E_a, which was expressed as Eq. (4) [19]:

$$\ln\left(\frac{d\alpha}{dt}\right) = \ln A + \ln f(\alpha) - \frac{E_a}{RT} \tag{4}$$

where, t is the reaction time of the pyrolysis (min); $d\alpha/dt$ is the sample conversion rate as a function of time; A is the pre-exponential factor (min^{-1}); $f(\alpha)$ is the kinetic mechanism function; T is the thermodynamic temperature (K); R is the universal gas constant ($R = 8.314\ J \cdot mol^{-1} \cdot K^{-1}$). In this case, α represents the conversion rate, which can be calculated using Eq. (5):

$$\alpha = \frac{W_i - W_t}{W_i - W_f} \tag{5}$$

where, W_i and W_f represent the initial and final masses of the sample during the catalytic pyrolysis reaction. W_t represents the mass at time t. E_a can be determined by fitting a linear relationship of $\ln(d\alpha/dt)$ versus $1/T$.

Additionally, the Kissinger–Akahira–Sunose (KAS) and Starink (STA) methods can be used to verify E_a, with their expressions shown in Eqs. (6) and (7) [20]:

$$\ln\left(\frac{\beta}{T^2}\right) = \ln\frac{AR}{E_K g(\alpha)} - \frac{E_K}{R}\cdot\frac{1}{T} \tag{6}$$

$$\ln\left(\frac{\beta}{T^{1.92}}\right) = \text{Constant} - 1.0008\frac{E_S}{R}\cdot\frac{1}{T} \tag{7}$$

where, β is the heating rate ($K \cdot min^{-1}$); E_K and E_S are the average E_a values calculated by the KAS and STA methods, respectively.

In order to further elucidate the pyrolysis mechanism, the Šesták–Berggren model was applied to calculate the A and $f(\alpha)$. Which was expressed as follows [21]:

$$f(\alpha) = (1-\alpha)^n \alpha^m [-\ln(1-\alpha)]^p \tag{8}$$

The model (Eq. (8)) can be seen as a unified form of f_1 to f_8 mechanism functions (Table 1), which mathematic expression is shown as Eq. (9):

$$\begin{pmatrix} f_1 \\ f_2 \\ f_3 \\ f_4 \\ f_5 \\ f_6 \\ f_7 \\ f_8 \end{pmatrix} = \begin{pmatrix} 1/2 & 0 & -1 & 0 \\ 1 & 0 & 0 & -1 \\ 1/n & 1 & 0 & 1-n \\ 1 & 0 & 0 & 1 \\ 1/n & 0 & 1-n & 0 \\ 1/n & 0 & 1 & 0 \\ 1 & n & 0 & 0 \\ 1 & n & m & p \end{pmatrix} \begin{pmatrix} 1 \\ \ln(1-\alpha) \\ \ln\alpha \\ \ln(-\ln(1-\alpha)) \end{pmatrix} \tag{9}$$

Furthermore, Eq. (8) can be logarithmically expressed as:

$$\ln\left(\frac{d\alpha}{dt}\right) + \frac{E_a}{RT} = \ln A + n\ln(1-\alpha) + m\ln\alpha + p\ln[-\ln(1-\alpha)] \tag{10}$$

where, E_a is the average activation energy calculated by the Friedman method ($kJ \cdot mol^{-1}$). At a certain heating rate, the independent parameters (n, m, p, and $\ln A$) are obtained by multiple linear regression of $\ln(1-\alpha)$, $\ln\alpha$, and $\ln[-\ln(1-\alpha)]$.

Table 1
Mechanism functions of kinetic for pyrolysis [22–25].

Number	Function name	Differential expression $f(\alpha)$
f_1	Parabola law	$\frac{1}{2}\alpha^{-1}$
f_2	Valensi 2-dimensional diffusion model	$[-\ln(1-\alpha)]^{-1}$
f_3	Avrami–Erofeev nuclei growth model	$\frac{1}{n}(1-\alpha)[-\ln(1-\alpha)]^{1-\alpha}$
f_4	Mampel unimolecular law	$-\ln(1-\alpha)$
f_5	Power law	$\frac{1}{n}\alpha$
f_6	Exponential law	$\frac{\alpha}{n}, n = 1,2$
f_7	Reaction order	$(1-\alpha)^n$
f_8	Šesták–Berggren function	$(1-\alpha)^n\alpha^m[-\ln(1-\alpha)]^p$
f_9	Brounstein–Ginstling 3-dimensional diffusion model	$\frac{3}{2}\left[(1-\alpha)^{-\frac{1}{3}}-1\right]^{-1}$
f_{10}	Zhuralev–Lesokin–Tempelman function	$\frac{3}{2}(1-\alpha)^{\frac{4}{3}}\left[(1-\alpha)^{-\frac{1}{3}}-1\right]^{-1}$
f_{11}	Jander diffusion model	$\frac{3}{n}(1-\alpha)^{1-\frac{1}{m}}\left[1-(1-\alpha)^{\frac{1}{m}}\right]^{-1}$ $m = 2,3$, $n = 1/2,2$
f_{12}	Anti-Jander counter diffusion model	$\frac{3}{2}(1+\alpha)^{\frac{2}{3}}\left[(1+\alpha)^{\frac{1}{3}}-1\right]^{-1}$

2.4. Characterization

Thermogravimetry (TG, TGA/DSC 3+, Mettler Toledo, Switzerland) was employed to study the pyrolysis process. Gas chromatography-mass spectrometry (GC-MS, QP2010, Shimadzu, Japan) was used to qualitatively identify the types of pyrolysis oils and gases. Scanning electron microscopy (SEM, SIGMA 300, Zeiss, Germany) was used to characterize the microstructure and morphology of the pyrolysis solids. X-ray diffraction (XRD, D/MAX-2500/PC, Rigaku, Japan) was used to study the crystalline structure and composition of the pyrolysis solids. To further reveal the reaction mechanism, thermogravimetric Fourier transform infrared spectroscopy–mass spectrometry (TG-FTIR-MS, Pyris1 & Nicolet6700, Thermo Fisher, American) and *in situ* Fourier transform infrared spectroscopy (*in-situ* FTIR, Nicolet iS50, Thermo Fisher) were employed to measure the real-time changes in chemical structures and functional groups during the pyrolysis process (Supplementary Material Text 2).

3. Results and Discussion

3.1. TG and DTG analysis

TG and DTG techniques were employed to analyze the Cu-free and Cu-assisted pyrolysis process of WPU. As shown in Fig. 2(a), (b), two significant mass loss stages were observed as the temperature increased from 453 to 833 K. During the 473–673 K stage, the majority of mass loss (approximately 60%) occurred. Further analysis of the DTG curve revealed that the maximum mass loss rate occurred in the temperature range of 593–633 K. This phenomenon may be mainly attributed to the cleavage of chemical bonds and the volatilization of low-molecular-weight compounds [26]. During the 673–833 K stage, the mass loss was approximately 13%. This result may be mainly attributed to the polyol backbone of the WPU and intermediates from the initial step pyrolyze and volatilize [27]. After exceeding 833 K, the TG curve leveled off, indicating the completion of the pyrolysis process. After the addition of Cu, as shown in Fig. 2(c), (d), only one significant mass loss stage was observed for Cu-assisted WPU as the temperature increased from 453 to 833 K. The TG curve also shifted toward a lower temperature range, reducing the initial decomposition temperature (T_i) of WPU from 473 to 453 K. These observed phenomena suggest that Cu may promote the initiation of pyrolysis and facilitate the cleavage of urethane bonds. Additionally, Cu can promote the pyrolysis process due to its excellent thermal conductivity, which enhances heat transfer [28].

To further reveal the effect of heating rates on the pyrolysis process of Cu-assisted WPU, the experimental data of Cu-free and Cu-assisted WPU pyrolysis for the initial temperature (T_i), final temperature (T_f), and the temperature at maximum reaction

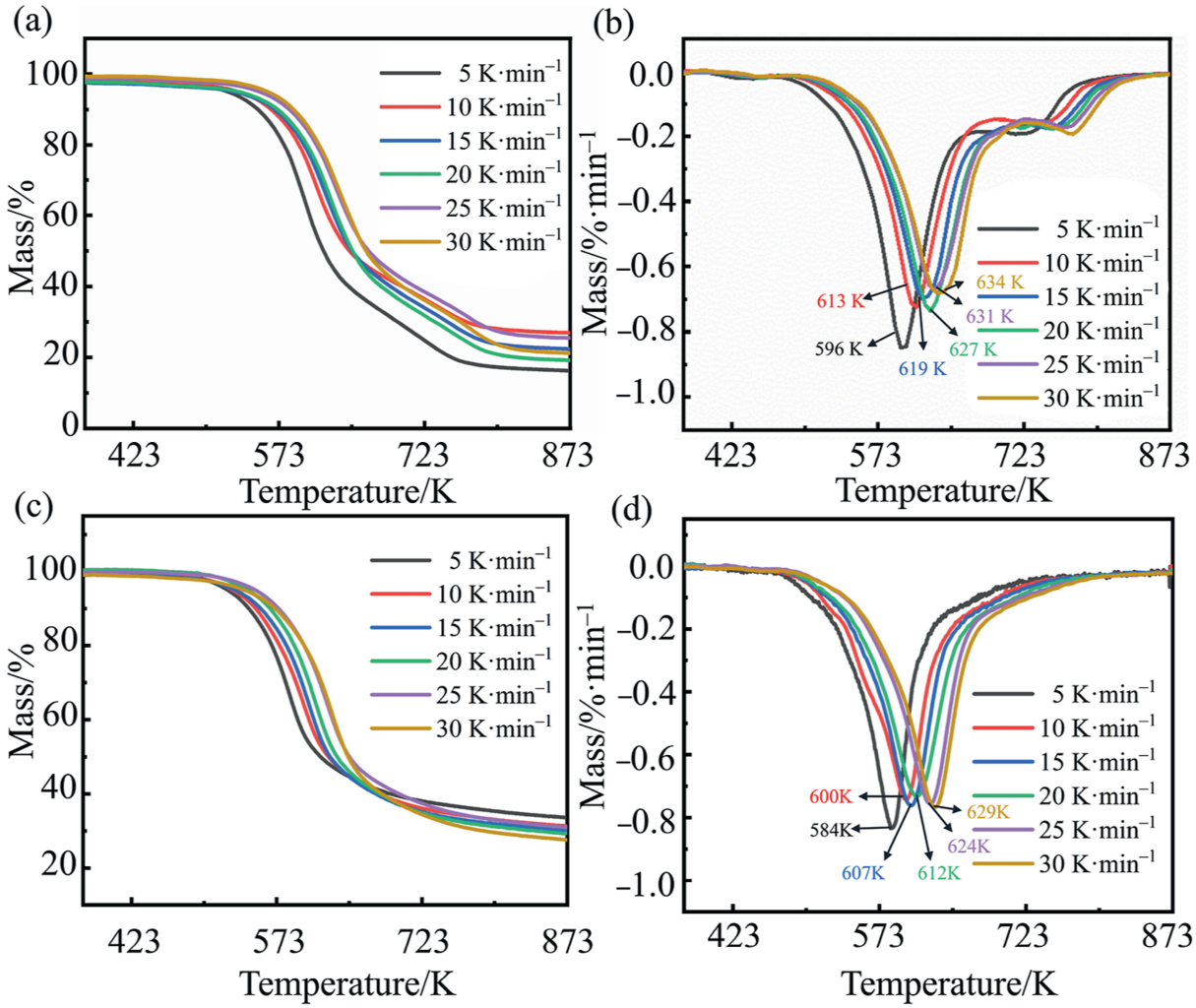

Fig. 2. The TG and DTG analysis of Cu-free (a, b) and Cu-assisted (c, d) WPU pyrolysis at heating rates from 5 to 30 K·min^{-1}.

speed (T_p) were given in Table S1. The results indicated that the T_i, T_p and T_f of the Cu-assisted WPU pyrolysis process were lower than those for WPU without Cu. With the increase in heating rate, the peak temperature of the degradation rate shifted toward higher temperatures. This phenomenon was caused by a mismatch between the actual heat transfer rate from the furnace to the sample and the programmed heating rate, which leaded to a decrease in the actual reaction rate [29]. Therefore, with the increase in heating rate, the pyrolysis curves shift toward high temperatures.

3.2. Kinetics analysis

To elucidate the mechanism of Cu-assisted pyrolysis, the kinetic parameters were calculated. As shown in Fig. 3(a), E_a was calculated by the method of Friedman. E_K and E_S were determined by the method of KAS and STA (Fig. S2). The high degree of linear fitting ($R^2 > 0.99$) at different heating rates confirmed the validity of the fitting results. Fig. 3(b) illustrated the E_a, E_K and E_S values at different α. It can be observed that the E_a values showed a fluctuating trend as the α increased from 0.05 to 0.60. The initial value of E_a was 126.09 kJ·mol^{-1}. The value of E_a increased to 136.81 kJ·mol^{-1} with α ranging from 0.05 to 0.3, which might have been caused by the cleavage of urethane bonds in WPU. The value of E_a dropped to 109.71 kJ·mol^{-1} as α reached 0.6. This may be due to the decomposition of polyols and isocyanates, which were broken down into small molecules products [11]. It can be observed that the E_a value increased sharply from 125.09 to 249.23 kJ·mol^{-1} when the α was higher than 0.65, which was related to the carbonization and dehydrogenation of the remaining pyrolysis residue. The average E_a for the entire pyrolysis process of WPU was 136.64 kJ·mol^{-1}. Moreover, the average values of E_K and E_S were 137.36 and 135.09 kJ·mol^{-1}. The consistency among E_a, E_K and E_S indicated that the method for accurately calculating E_a was suitable and the obtained E_a value was reliable. When Cu was added for pyrolysis of WPU, the calculated average E_a decreased compared to that of the Cu-free WPU determined in this work (Fig. S3), as well as to the values reported in previous studies on WPU pyrolysis [13]. This proved that the addition of Cu effectively reduced the E_a and promoted the occurrence and progress of the pyrolysis reaction.

To further elucidate the pyrolysis mechanism function, the Šesták–Berggren model was applied to calculate A and $f(\alpha)$. The model was not affected by the assumed model formula, avoiding errors introduced by the hypothetical mechanism function [30]. As a result, the calculation results were more realistic. Table 2 showed the fitting results of the Šesták–Berggren model. The high correlation coefficients ($R^2 > 0.9$) demonstrated the reliability of the Šesták–Berggren model calculations. The fundamental kinetic equation for the Cu-assisted pyrolysis of WPU was shown in the following formula:

$$\frac{d\alpha}{dt} = 8.99 \times 10^9 \times \left[(1-\alpha)^{-0.8}\alpha^{9.19}\left(-\ln(1-\alpha)^{-9.5}\right)\right] \exp\left(-\frac{136636}{8.314 \times T}\right) \quad (11)$$

To verify the accuracy of $f(\alpha)$, the commonly used models f_9–f_{12} in Table 1 were employed. The fitting results (Fig. S4) showed that the mechanism functions f_9–f_{12} did not satisfy the requirements of $R^2 \geq 0.95$ and $\left|(E_a - E_{a(f_9-f_{12})})/E_a\right| \leq 0.15$. Therefore, these mechanism functions cannot accurately describe the pyrolysis behavior.

To illustrate the effects of mechanism functions during Cu-assisted pyrolysis process of WPU, the normalized contributions of the Šesták–Berggren model were analyzed (Fig. 4). In the Šesták–Berggren model, $m \ln \alpha$, $n \ln(1-\alpha)$, and $p \ln(-\ln(1-\alpha))$ represented the diffusion, phase boundary and nucleation reaction mechanisms, respectively. A positive contribution value indicated that the mechanism facilitated the pyrolysis reaction, whereas a negative value suggested that the mechanism inhibited the pyrolysis reaction. In the initial stage of pyrolysis ($\alpha < 0.13$), the

Table 2
Fitting results of Šesták–Berggren model for Cu-assisted WPU.

β/K·min^{-1}	n	m	p	ln A	R^2
5	−1.1076	11.3933	−11.5238	23.2049	0.9663
10	−1.0910	10.6541	−10.8279	23.0882	0.9859
15	−0.8445	9.5064	−9.7087	22.9571	0.9822
20	−0.4234	7.3473	−7.8105	22.2899	0.9602
25	−0.8380	8.8179	−9.1949	23.8711	0.9902
30	−0.5772	7.4168	−7.8682	22.0213	0.9901
Average	−0.8136	9.1893	−9.4890	22.9054	0.9791

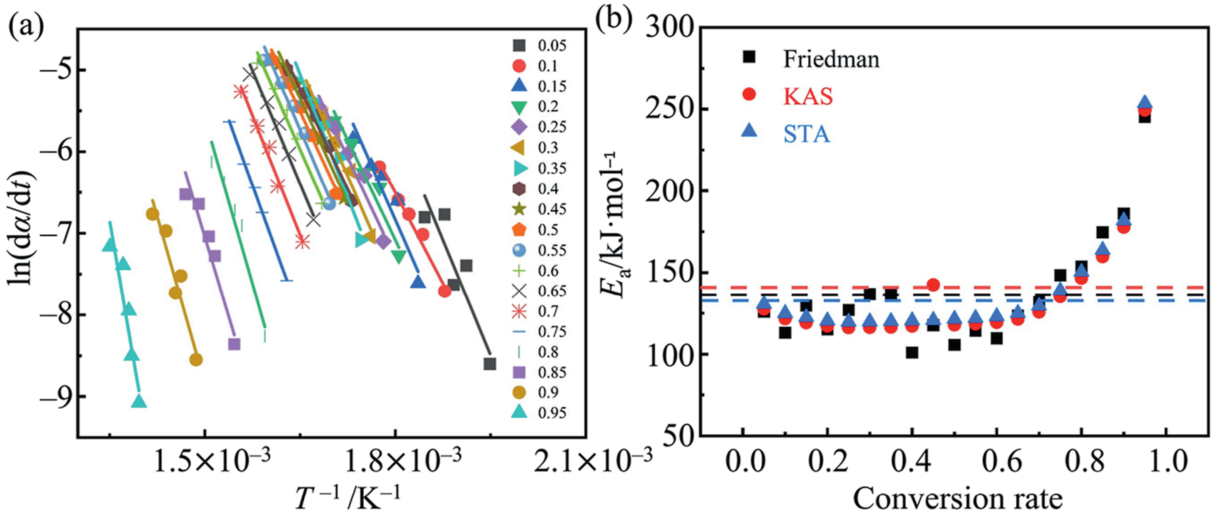

Fig. 3. (a) Linear fitting results of ln(dα/dt) *versus* 1/T using the Friedman method at different reaction fractions for Cu-assisted WPU pyrolysis; (b) E_a calculated by the Friedman, KSA, and STA methods based on the experimental data of Cu-assisted WPU.

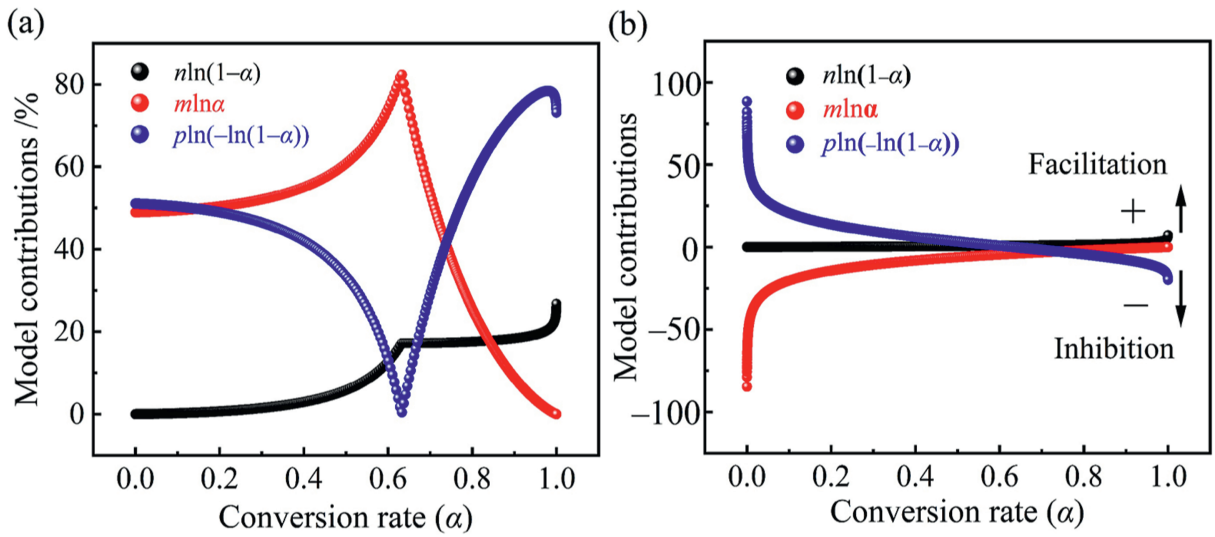

Fig. 4. (a) Normalized contributions and (b) contributions at different reaction fractions (α) of Cu-assisted WPU.

normalized contribution values of $m \ln \alpha$ and $p \ln(-\ln(1-\alpha))$ were relatively large, whereas that of $n \ln(1-\alpha)$ was extremely small and approximately zero. This showed that this stage was mainly controlled by diffusion and nucleation reactions, while the phase boundary reaction did not play a significant role. The positive value of $p \ln(-\ln(1-\alpha))$ suggested that the nucleation reaction promoted the pyrolysis, while the negative value of $m \ln \alpha$ suggested that the diffusion reaction was the dominant rate-control step. The accumulation of the old phase facilitated the continuous generation of new phase [31], thereby promoting the initiation and progression of the nucleation reaction. However, since gas channels had not yet formed during the initial stage of pyrolysis, and the addition of Cu may hinder their formation, the escape of pyrolysis oil and gas was obstructed, exacerbating the suppression of the diffusion reaction. In the intermediate stage of pyrolysis ($0.13 < \alpha < 0.63$), the diffusion reaction remained the dominant reaction in this stage. The absolute values of $p \ln(-\ln(1-\alpha))$ and $m \ln \alpha$ decreased, indicating that both the promoting effect of nucleation reactions and the inhibiting effect of diffusion reactions were gradually weakened. This was caused by the consumption of materials and the generation of gas channels [31]. Additionally, the value of $n \ln(1-\alpha)$ increased, indicating that the phase boundary reaction played a role. This might be attributed to the increased aggregation of WPU particles [32]. In the final stage of pyrolysis ($\alpha > 0.63$), the value of $p \ln(-\ln(1-\alpha))$ changed to negative and the value of $m \ln \alpha$ gradually approached zero because of the depletion of reaction substrate. Meanwhile, the value of $m \ln \alpha$ gradually approached zero, indicating that the inhibitory effect of diffusion-controlled reactions on the Cu-assisted pyrolysis of WPU had almost completely disappeared.

3.3. Pyrolysis products analysis

To analyze the influence of Cu addition on the pyrolysis products, a yield analysis of the three-phase pyrolysis products at different heating rates was conducted. As shown in Fig. 5, the addition of Cu increased the average pyrolysis solid yield across different heating rates, rising from 23.9% in the Cu-free WPU to 30.56% in the Cu-assisted WPU. Meanwhile, the average yields of pyrolysis oil and gas were slightly reduced in the Cu-assisted WPU, suggesting that the addition of Cu influenced the distribution of pyrolysis products. For both Cu-free and Cu-assisted WPU,

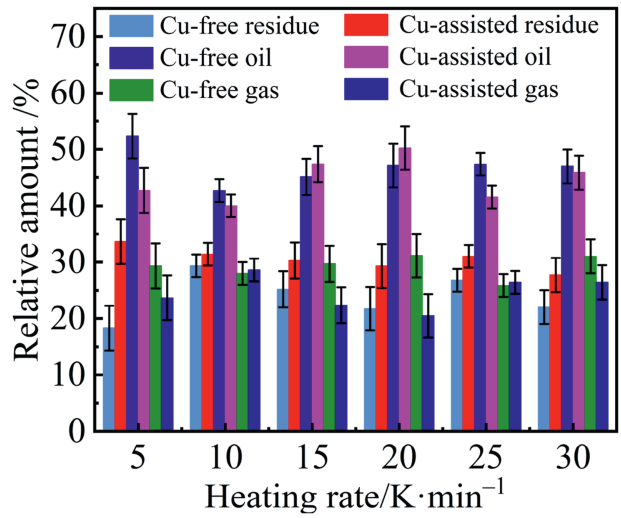

Fig. 5. The proportion of pyrolysis products of Cu-free and Cu-assisted WPU at different heating rates (5–30 K·min^{-1}), with a final temperature of 873 K under an argon flow rate of 50 ml·min^{-1}.

pyrolysis oil was the predominant product, with an average yield across different heating rates of approximately 44.62% and 46.9%, respectively. Furthermore, the change in heating rate had no significant effect on the relative proportions of the three-phase pyrolysis products during pyrolysis.

GC-MS analysis was performed to explore the effect of Cu on the composition of pyrolysis oil and gas (Tables S2–S3). It can be seen that the pyrolysis gas and pyrolysis oil contained 12 and 21 components, respectively. Aniline and its derivatives, alkanes, alkenes, and polyols were the main species in the pyrolysis products. Compared with previous reports, the content of aniline and its derivatives increased, while that of heterocyclic compounds decreased in the pyrolysis oil. Cu promoted the decarboxylation of intermediate isocyanates, making the decomposition pathway more inclined toward aniline formation [33]. Cu can promote the cleavage of C–Cl and C–F bonds, reducing fluorochlorinated compounds in the pyrolysis gas [34]. These results showed that the addition of Cu inhibited the formation of harmful substances in the pyrolysis oil and gas, thereby simplifying their composition.

To further analyze the effect of Cu on WPU, the morphology and composition of the pyrolysis residues were studied using SEM and XRD. As shown in Fig. S5(a) and (b), the pyrolysis residues of WPU appeared as black solid with smooth and flat surfaces, exhibiting a stacked lamellar structure without obvious pore distribution on the surface. The main elemental mass composition of the solid residues from pyrolysis consists of carbon (78.49%), oxygen (10.6%), nitrogen (8.57%), and hydrogen (2.34%). As shown in Fig. S5(c), the XRD results of the pyrolysis residue revealed two diffraction peaks at 26° and 44°, corresponding to the (0 0 2) and (1 0 0) crystal planes of graphite (JCPDS 99-0057), respectively. This suggested that the pyrolysis residue possessed a graphitized structure with low crystallinity.

3.4. Mechanism

TG-FTIR analysis was performed for real-time analysis of pyrolysis oil and gas. As shown in Fig. 6, the characteristic bands appeared at 2800–3100, 2250–2400, 1400–1700, 1000–1300, and 710–730 cm^{-1}. When the temperature exceeded 523 K, the characteristic bands of –N=C=O group observed at 2200–2400 cm^{-1} indicated the onset of WPU decomposition. The peaks observed around 720 and 1006 cm^{-1} corresponded to the stretching vibrations of C–Cl and C–F, respectively [13,35]. This suggests that CFC–11 may have undergone partial thermal degradation. After the temperature rose above 573 K, the C–H bands of unsaturated carbons exhibited stretching vibrations at wavenumbers of 3000–3100 cm^{-1}. Stretching vibration bands of $-CH_3$ and $-CH_2-$ appeared at 2980 cm^{-1} and 2930 cm^{-1}, confirming the production of alkanes. The absorption bands at 1600–1700 cm^{-1} were attributed to the stretching vibration of C=O in carboxylic acids and the C=C in alkenes. The bands observed at 1200–1300 cm^{-1} were attributed to the presence of C–O in polyols. The bands at 1000–1200 cm^{-1} were derived from the asymmetric stretching vibrations of C–O–C in ethers [10]. At temperatures above 623 K, the absorption bands of the benzene ring were detected at

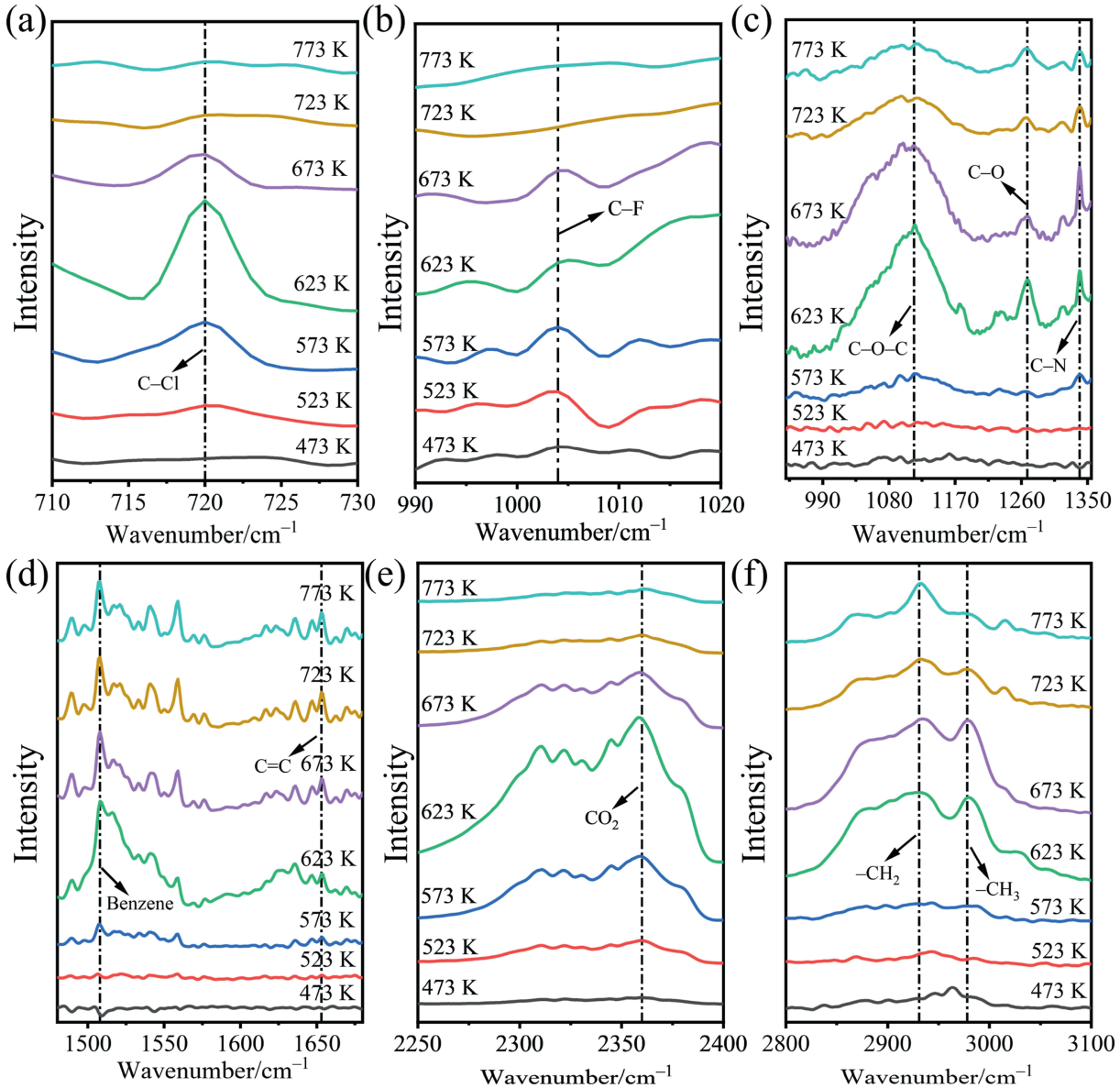

Fig. 6. TG-FTIR analysis of pyrolysis gas and oil at different temperatures in selected wavenumber regions: (a) 710–730 cm^{-1}, (b) 990–1020 cm^{-1}, (c) 990–1350 cm^{-1}, (d) 1500–1700 cm^{-1}, (e) 2250–2400 cm^{-1} and (f) 2800–3100 cm^{-1}.

1400–1600 cm^{-1}. Meanwhile, the absorption peaks located at 1310–1330 cm^{-1} could be attributed to the stretching vibration of C–N in amine compounds. This result confirmed the formation of aniline and its derivatives. The peaks at 2300–2400 cm^{-1} suggested the formation of CO_2. Compared with previous literature reports [13], it can be observed that the temperatures at which the characteristic bands of Cu-assisted WPU appear are generally lower than those without Cu. This phenomenon may be caused by the *in-situ* catalysis of Cu. The Cu particles directly transfer the electrons from conduction band to WPU, which can weaken the strength of C–O bond in the carbamate and promote the pyrolysis. *In-situ* FTIR was further employed to investigate the structural evolution of pyrolysis solid during the pyrolysis process. As shown in Fig. S6, when the temperature was below 463 K, no significant thermal decomposition of WPU was observed, which was consistent with the TG-FTIR results. When the temperature exceeds 463 K, the absorption peak at 1540 cm^{-1} corresponding to the –NH–COO– groups began to decrease, suggesting the cleavage of urethane bonds in WPU and the onset of pyrolysis. Meanwhile, a characteristic peak at 2273 cm^{-1} appeared, suggesting the formation of –NCO groups. As the temperature continues increased, most of the absorption peaks gradually decreased in intensity, implying that WPU decomposed drastically, which was consistent with the TG results.

TG-MS was employed to further elucidate the catalytic mechanism of Cu. Fig. 7 illustrated the release intensity of propylene, propane, ethanol, and aniline and its derivatives as a function of temperature. The peak intensity was positively correlated with the content of pyrolysis products. Peaks of aniline, *o*-toluidine, and 2,3-dimethylaniline were detected at temperatures below 723 K. In contrast, previous reports showed that these peaks were only observed in Cu-free WPU when the temperature exceeded 723 K [13,36]. Meanwhile, small molecule products (propylene, propane, and ethanol) were generated earlier because the active sites provided by Cu interacted with C–O single bonds in the carbamate and ethylene glycol, reducing their decomposition activation energy and facilitating the decomposition reaction at lower temperatures. This was consistent with the previously calculated kinetic results. Furthermore, the addition of Cu increased the generation of aniline, *o*-toluidine, and 2,3-dimethylaniline at 723–873 K. This could be attributed to the Ullmann C–N coupling caused by Cu, which facilitated C–N coupling, leading to an increased content of aniline and its derivatives [37]. As shown in Fig. S7, signals at *m*/*z* 76, 134 and 208 were attributed to the evolution of propylene glycol, 2-(2-hydroxypropoxy)-1-propanol, and tetraethyleneglycol monomethyl ether, respectively. Furthermore, signals at *m*/*z* 198, 250 and 258 were attributed to the evolution of 4,4′-diaminodiphenylmethane, 4′-diphenylmethane diisocyanate, and (methylenebis-(4,1-phenylene)) dicarbamic acid, respectively. This indicated that Cu not only accelerated the decomposition of WPU but also effectively increased the relative content of aniline and its derivatives.

Based on the results of kinetic and pyrolysis product analysis, the mechanism of Cu in the pyrolysis of WPU was proposed. As shown in Fig. S8, during the initial stage of pyrolysis (<523 K), co-pyrolysis of Cu with WPU reduced the activation energy of the reaction and promoted the cleavage of urethane bonds. The active sites on the surface of Cu atoms adsorbed and weakened the C–O bonds in urethane groups. Heating led to bond cleavage, producing isocyanates and polyols. During the intermediate stage of pyrolysis (523–773 K), due to sufficient energy supply, the random cleavage of chemical bonds and the recombination of radicals could form various pyrolysis products. At this stage, Cu exerted a significant influence on the pyrolysis process and product composition. Cu interacted with the π-electrons in aromatic structures, leading to their cleavage into small molecular products, reducing the likelihood of further rearrangement into polycyclic or heterocyclic compounds [38]. Additionally, Cu promoted the cleavage of C–*X* (*X* = Cl, F) bonds through orbital-level interactions. Its partially filled 3d orbitals stabilized the lone pairs of halogen atoms *via* back-donation, while the 4s orbital donated electron density into the antibonding orbital of the C–*X* bond [39,40]. These combined effects weakened the C–*X* bond, facilitating its dissociation. The resulting halide ions were immobilized as stable Cu–*X* complexes

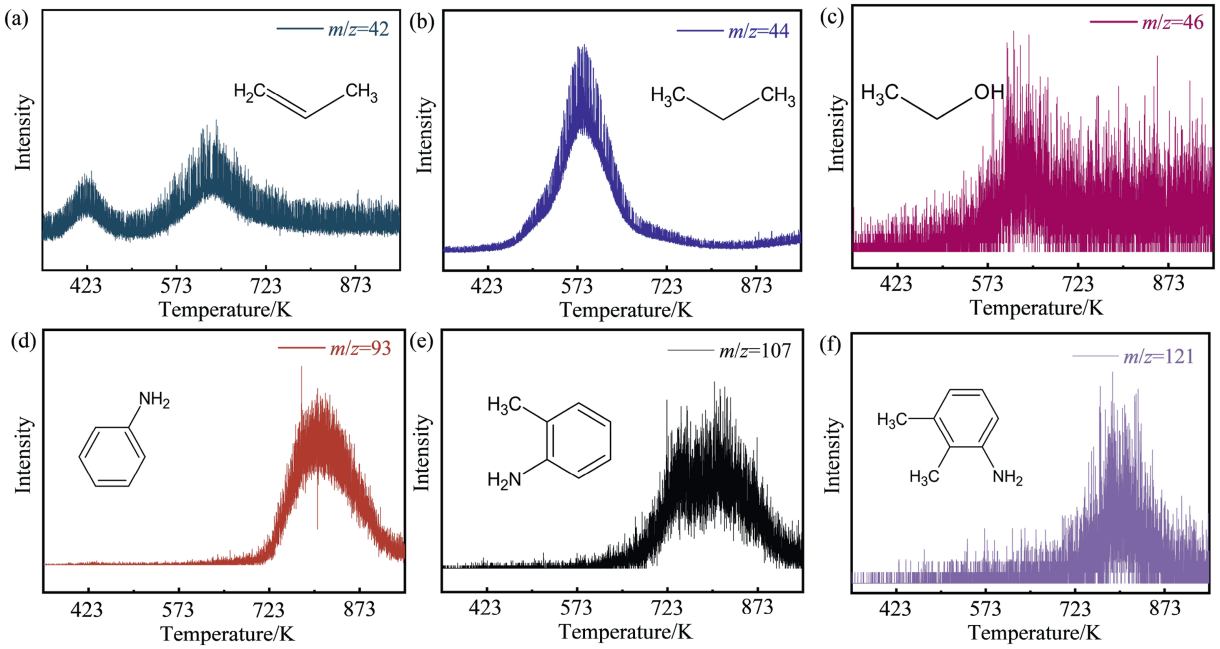

Fig. 7. TG-MS curves of the thermal decomposition of Cu-assisted WPU: (a) propene (*m*/*z* = 42), (b) propane (*m*/*z* = 44), (c) ethanol (*m*/*z* = 46), (d) aniline (*m*/*z* = 93), (e) *o*-toluidine (*m*/*z* = 107), (f) 2,3-dimethylaniline (*m*/*z* = 121).

in the pyrolysis residue, thereby suppressing the release of halogenated compounds into the pyrolysis gases [41,42]. During the final stage of pyrolysis (>773 K), the decomposition of WPU was nearly completed. At this stage, the reaction process was controlled by dehydrogenation and carbonization, which were slightly affected by Cu particles.

4. Conclusions

In this study, the pyrolysis behavior of Cu-assisted WPU was investigated in depth through mechanistic function analysis and *in situ* coupling online monitoring. The Cu-assisted mechanism function of WPU was determined by Šesták–Berggren model and described as: $d\alpha/dt = 8.99 \times 10^9 \times \left[(1-\alpha)^{-0.8}\alpha^{9.19}\left(-\ln(1-\alpha)^{-9.5}\right)\right]\exp(-136636/8.314 \times T)$. This indicated that the pyrolysis reaction mechanism function was not governed by a simple single mechanism, but rather by a combined mechanism of diffusion, nucleation, and phase boundary reactions. The average E_a of the reaction was calculated to be 136.64 $kJ \cdot mol^{-1}$. Moreover, Cu has catalytic effects on thermal decomposition, causing a decrease in the initial, peak, and final temperature of pyrolysis. Cu not only enhanced the ethanol content in the final products but also suppressed the presence of fluorine–chlorine compounds in the pyrolysis gases. Cu could form chemical bonds with halogen atoms and facilitate electron transfer, thereby promoting the cleavage of C–X (X = F, Cl) bonds and enhancing the dehalogenation process. Additionally, Cu addition effectively increased the proportion of aniline and its derivatives, significantly decreasing the formation of harmful heterocyclic compounds. Therefore, the presence of Cu could facilitate the pyrolysis of WPU and improve the manageability of the resulting products for subsequent disposal.

CRediT Authorship Contribution Statement

Houyuan Jia: Writing – original draft, Methodology, Investigation, Conceptualization. Jiahui Wang: Methodology, Investigation. Chunyan Feng: Methodology, Investigation. Siyi Xu: Investigation. Ruitong Gao: Writing – review & editing, Methodology, Funding acquisition, Conceptualization. Hui Du: Supervision, Resources, Funding acquisition.

Declaration of Competing Interest

The authors declare that they have no known competing financial interests or personal relationships that could have appeared to influence the work reported in this paper.

Acknowledgements

This work was supported by the Natural Science Foundation of Shandong Province (ZR2022QE042); China Postdoctoral Science Foundation (2023M741856); and the National Natural Science Foundation of China (52172093).

Supplementary Material

Supplementary data to this article can be found online at https://doi.org/10.1016/j.cjche.2025.08.014.

References

[1] A. Delavarde, G. Savin, P. Derkenne, M. Boursier, R. Morales-Cerrada, B. Nottelet, J. Pinaud, S. Caillol, Sustainable polyurethanes: toward new cutting-edge opportunities, *Prog. Polym. Sci.* 151 (2024) 101805.
[2] H.R. Wang, T. Li, J. Li, R.H. Zhao, A. Ding, F.J. Xu, Structural engineering of polyurethanes for biomedical applications, *Prog. Polym. Sci.* 151 (2024) 101803.
[3] K. Jagodzińska, C. Garcia Lopez, W.H. Yang, P.G. Jönsson, T. Pretz, K. Raulf, Characterisation of excavated landfill waste fractions to evaluate the energy recovery potential using Py-GC/MS and ICP techniques, *Resour. Conserv. Recycl.* 168 (2021) 105446.
[4] Polyurethane Market Size - Industry Report on Share, Growth Trends & Forecasts Analysis (2025 - 2030), 2025. https://www.mordorintelligence.com/industry-reports/polyurethane-market.
[5] G.Y. Chen, T.C. Liu, P.P. Luan, N. Li, Y.N. Sun, J.Y. Tao, B.B. Yan, Z.J. Cheng, Distribution, migration, and removal of N-containing products during polyurethane pyrolysis: a review, *J. Hazard. Mater.* 453 (2023) 131406.
[6] C. Chang, Y.F. Jiang, Y.C. Lin, K. Fu, C.B. Xu, S.Q. Zhao, Glycolysis of waste polyurethane foam for preparing recycled polymer materials: optimization and techno-economic evaluation, *Chem. Eng. J.* 507 (2025) 160583.
[7] N. Wybo, E. Cherasse, A. Duval, L. Avérous, Unlocking sustainable, aromatic, and versatile materials through transurethanization: development of non-isocyanate polyurethanes from lignins, *J. Mater. Chem. A* 13 (16) (2025) 11557–11572.
[8] M.A. Alreshidi, K.K. Yadav, G. Shoba, A. Gacem, S. Padmanabhan, T. Vinod Kumar, A.M. Fallatah, J.K. Bhutto, F.M. Aldosari, M. Alam, M.A. Abo El-Khair, P. Tamizhdurai, A. Subramani, V.L. Mangesh, R. Kumaran, Advancements in the production methods and recycling of multilayer plastics with sustainable applications: a comprehensive review, *Chem. Eng. J.* 515 (2025) 163633.
[9] Z.T. Yao, S.Q. Yu, W.P. Su, D.D. Wu, J. Liu, W.H. Wu, J.H. Tang, Probing the combustion and pyrolysis behaviors of polyurethane foam from waste refrigerators, *J. Therm. Anal. Calorim.* 141 (3) (2020) 1137–1148.
[10] S.M. Choi, E.J. Shin, S.M. Zo, M.R. Kummara, C.M. Kim, A. Kumar, H.J. Bae, A. Sood, S.S. Han, Development of scalable elastic gelatin hydrogel films crosslinked with waterborne polyurethane for enhanced mechanical properties and strain recovery, *Gels* 11 (1) (2025) 49.
[11] X.J. Tang, Z.H. Chen, J.Y. Liu, Z.Y. Chen, W.M. Xie, F. Evrendilek, M. Buyukada, Dynamic pyrolysis behaviors, products, and mechanisms of waste rubber and polyurethane bicycle tires, *J. Hazard. Mater.* 402 (2021) 123516.
[12] J. Oenema, H.R. Liu, N. de Coensel, A. Eschenbacher, R. van de Vijver, J.J. Weng, L. Li, C.J. Wang, K.M. van Geem, Review on the pyrolysis products and thermal decomposition mechanisms of polyurethanes, *J. Anal. Appl. Pyrolysis* 168 (2022) 105723.
[13] S.Y. Xu, E.H. Liu, R.T. Gao, H. Du, Z.J. Chen, Q. Sun, Z.M. Xu, Insight into waste polyurethane pyrolysis pathways: mechanism functions analysis and *in situ* coupling online monitoring, *J. Anal. Appl. Pyrolysis* 177 (2024) 106301.
[14] D. Laishram, S.B. Kim, S.Y. Lee, S.J. Park, Advancements in biochar as a sustainable adsorbent for water pollution mitigation, *Adv. Sci. (Weinh)* 12 (19) (2025) e2410383.
[15] F. Niu, Z.Q. Wu, D. Chen, Y.X. Huang, V.V. Ordomsky, A.Y. Khodakov, K.M. van Geem, State-of-the-art and perspectives of hydrogen generation from waste plastics, *Chem. Soc. Rev.* 54 (10) (2025) 4948–4972.
[16] R.T. Gao, B.Y. Liu, L. Zhan, J. Guo, J. Zhang, Z.M. Xu, Catalytic effect and mechanism of coexisting copper on conversion of organics during pyrolysis of waste printed circuit boards, *J. Hazard. Mater.* 403 (2021) 123465.
[17] C.L. Liu, Y.X. Li, D.K. Fan, P.F. Zhu, Y. Liu, L. Chao, C.B. Zhou, B. Yao, Y.W. Zhang, J. J. Dai, *In situ* catalytic pyrolysis of oily sludge using coal gangue char to produce naphthalene-rich oil and hydrogen-rich gas, *Chem. Eng. J.* 508 (2025) 160953.
[18] Y. Liu, A. A. Siyal, C.B. Zhou, C.L. Liu, J. Fu, Y.W. Zhang, B. Yao, L. Chao, H.M. Yun, J.J. Dai, X.T. Bi, Microwave co-pyrolysis of industrial sludge and waste biomass: product valorization and synergistic mechanisms, *Chem. Eng. J.* 485 (2024) 150032.
[19] Z.F. Wang, X.B. Long, W.L. Yao, W.C. Zhang, J.N. Yang, Study on the kinetics and mechanism of thermal decomposition of bisphenol A-type polyarylates, *J. Anal. Appl. Pyrolysis* 188 (2025) 107040.
[20] X.Y. Chen, D. Cai, Y.M. Yang, Y.H. Sun, B.H. Wang, Z.T. Yao, M.Q. Jin, J. Liu, M. Reinmöller, S.L. Badshah, A. Magdziarz, Pyrolysis kinetics of bio-based polyurethane: evaluating the kinetic parameters, thermodynamic parameters, and complementary product gas analysis using TG/FTIR and TG/GC-MS, *Renew. Energy* 205 (2023) 490–498.
[21] J. Šesták, G. Berggren, Study of the kinetics of the mechanism of solid-state reactions at increasing temperatures, *Thermochim. Acta* 3 (1) (1971) 1–12.
[22] J. Málek, The kinetic analysis of non-isothermal data, *Thermochim. Acta* 200 (1992) 257–269.
[23] J. Málek, J.M. Criado, A simple method of kinetic model discrimination. Part 1. Analysis of differential non-isothermal data, *Thermochim. Acta* 236 (1994) 187–197.
[24] J. Málek, A computer program for kinetic analysis of non-isothermal thermoanalytical data, *Thermochim. Acta* 138 (2) (1989) 337–346.
[25] J.M. Criado, J. Málek, A. Ortega, Applicability of the master plots in kinetic analysis of non-isothermal data, *Thermochim. Acta* 147 (2) (1989) 377–385.
[26] M. Zeller, D. Merz, L. Weigel, S. Tavakkol, D. Stapf, TG-FTIR investigations of the pyrolysis of polyurethanes: quantitative carbon dioxide tracing,

decomposition mechanisms, products and mass balances for advanced recycling, *J. Anal. Appl. Pyrolysis* 188 (2025) 107048.
[27] X. Xiao, B. Jiang, J. Li, S.N. Amirkhanian, F.P. Xiao, Pyrolysis optimization for sustainable down-cycling flexible polyurethane foam in asphalt industry, *Resour. Conserv. Recycl.* 206 (2024) 107608.
[28] W.J. Liu, K. Tian, H. Jiang, X.S. Zhang, H.S. Ding, H.Q. Yu, Selectively improving the bio-oil quality by catalytic fast pyrolysis of heavy-metal-polluted biomass: take copper (Cu) as an example, *Environ. Sci. Technol.* 46 (14) (2012) 7849–7856.
[29] J.O. Jaber, S.D. Probert, Pyrolysis and gasification kinetics of Jordanian oil-shales, *Appl. Energy* 63 (4) (1999) 269–286.
[30] J.F. Xiao, R.T. Gao, L. Zhan, Z.M. Xu, Unveiling the control mechanism of the carbothermal reduction reaction for waste Li-ion battery recovery: providing instructions for its practical applications, *ACS Sustainable Chem. Eng.* 9 (28) (2021) 9418–9425.
[31] D. Filip, D. Macocinschi, S. Vlad, Thermogravimetric study for polyurethane materials for biomedical applications, *Compos. Part B Eng.* 42 (6) (2011) 1474–1479.
[32] H. Jin, Q.G. Xiong, X.L. Zhang, Y.N. Zhang, ACS sustainable chemistry & engineering virtual special issue: thermal and catalytical chemical conversions of plastic wastes for sustainable production of energy, fuels, and chemicals, *ACS Sustainable Chem. Eng.* 11 (21) (2023) 7924–7926.
[33] Y.A. Liu, X.B. Liao, H. Chen, Recent progress in radical decarboxylative functionalizations enabled by transition-metal (Ni, Cu, Fe, co or Cr) catalysis, *Synthesis* 53 (1) (2021) 1–29.
[34] V.I. Kovalchuk, J.L. D'Itri, Catalytic chemistry of chloro- and chlorofluorocarbon dehalogenation: from macroscopic observations to molecular level understanding, *Appl. Catal. Gen.* 271 (1–2) (2004) 13–25.
[35] Y.C. Lu, L.J. Yin, W. Li, N.Y. Ning, M. Tian, W.C. Wang, Novel environmentally friendly dipping system for aramid fibers with strong interfacial adhesion and good storage stability, *Ind. Eng. Chem. Res.* 64 (12) (2025) 6550–6560.
[36] G. Moroi, Influence of ion species on the thermal degradation of polyurethane interaction products with transition metal ions, *J. Anal. Appl. Pyrolysis* 71 (2) (2004) 485–500.
[37] F. Monnier, M. Taillefer, Catalytic C-C, C-N, and C-O Ullmann-type coupling reactions: copper makes a difference, *Angew. Chem. Int. Ed.* 47 (17) (2008) 3096–3099.
[38] Y. Shen, C.J. Liu, C.H. Cui, H.R. Ren, M.M. Gu, H.R. Liu, Z.Y. Zhou, F. Qi, Effect of Cu-modified HZSM-5 zeolites on catalytic pyrolysis of lignin to producing aromatic hydrocarbons, *Fuel* 361 (2024) 130719.
[39] Z.W. Xiao, K.Z. Du, W.W. Meng, D.B. Mitzi, Y.F. Yan, Chemical origin of the stability difference between copper(I)- and silver(I)-based halide double perovskites, *Angew. Chem. Int. Ed.* 56 (40) (2017) 12107–12111.
[40] X.P. Sun, Symmetry analysis in mechanistic studies of nucleophilic substitution and β-elimination reactions, *Symmetry* 2 (1) (2010) 201–212.
[41] A.J. Thillman, E.C. Kill, A.N. Erickson, D. Wang, Visible-light-driven catalytic dehalogenation of trichloroacetic acid and α-halocarbonyl compounds: multiple roles of copper, *ACS Catal.* 15 (5) (2025) 3873–3881.
[42] R.H. Lin, A.P. Amrute, J. Pérez-Ramírez, Halogen-mediated conversion of hydrocarbons to commodities, *Chem. Rev.* 117 (5) (2017) 4182–4247.